Electrochemical Impedance Imaging via the Distribution of Diffusion Times

Juhyun Song[1] and Martin Z. Bazant[1,2,*]

[1]*Department of Chemical Engineering, Massachusetts Institute of Technology, Cambridge, Massachusetts 02139, USA*
[2]*Department of Mathematics, Massachusetts Institute of Technology, Cambridge, Massachusetts 02139, USA*

We develop a mathematical framework to analyze electrochemical impedance spectra in terms of a distribution of diffusion times (DDT) for a parallel array of random finite-length Warburg (diffusion) or Gerischer (reaction-diffusion) circuit elements. A robust DDT inversion method is presented based on complex nonlinear least squares regression with Tikhonov regularization and illustrated for three cases of nanostructured electrodes for energy conversion: (i) a carbon nanotube supercapacitor, (ii) a silicon nanowire Li-ion battery, and (iii) a porous-carbon vanadium flow battery. The results demonstrate the feasibility of nondestructive "impedance imaging" to infer microstructural statistics of random, heterogeneous materials.

In pursuit of a higher power and energy density as well as a longer lifetime, electrochemical energy systems increasingly employ hierarchical nanostructured materials [1–4]: Battery electrodes consist of nanoparticles [5–10]; supercapacitor electrodes are full of nanopores [11–15]; and in fuel cells [16–19] and flow batteries [20–22] electrolytes flow through nanoporous electrodes. The nanoscale diffusion lengths in such materials render the low-frequency transition from infinite-length Warburg impedance, scaling as $(i\omega)^{-1/2}$, where ω is the applied frequency [23,24], to finite-length behavior, either resistive or capacitive, now fully accessible to electrochemical impedance spectroscopy [25–27]. Nanostructured materials thus present the opportunity to exploit diffusion-related impedance features to quantitatively probe their internal structure. Conventional finite-length diffusion circuit elements are available to capture the transition, scaling as $\tanh(\sqrt{i\tau\omega})/\sqrt{i\tau\omega}$ for transmissive diffusion [28–30] and $\coth(\sqrt{i\tau\omega})/\sqrt{i\tau\omega}$ for bounded diffusion [26,31], where τ is the characteristic diffusion time, and variants have been derived for nonplanar geometries, such as cylindrical, spherical, and rectangular shapes [27,32]. When a charge transfer reaction takes place simultaneously along with diffusion, their Gerischer-type derivatives are obtained by replacing $\sqrt{i\tau\omega}$ with $\sqrt{\tau(k+i\omega)}$, where k is the apparent first-order kinetic constant [25,33–35]. Identical expressions are also used to model the impedance of porous electrodes, where τ becomes the charging time of the RC transmission line representing the pore resistors and double-layer capacitors [36,37].

Since conventional models assume constant material properties and simple geometries, experimental Nyquist plots often exhibit large deviations, such as a depressed Warburg arc for transmissive diffusion [38–40] or inclined capacitive rays for bounded diffusion [41–47]. The most common heuristic approach to describe such deviations is the constant phase element, scaling as $(i\omega)^{-\alpha}$, where $0 < \alpha < 1$, placed in various circuit arrangements, which is commonly rationalized by surface inhomogeneity [46–48]. While α is usually left as a fit parameter, there are microscopic morphology models to predict its value [49–51]. Another approach is the phenomenological modification of the conventional models by a fractional exponent, e.g., $\coth(i\tau\omega)^{\beta/2}/(i\tau\omega)^{\beta/2}$ for planar bounded diffusion, where $0 < \beta < 1$ [23,52–55], which could be attributed to surface roughness [41,56–58], hierarchical structures in porous electrodes [59], anomalous diffusion in disordered materials [57,60,61], or anisotropic diffusion in battery particles [32].

For many nanostructured materials, nonideal diffusion impedance is also attributable to the inherent geometrical randomness, such as particle size distribution in batteries, pore size distribution in capacitors, tortuosity distribution in membranes and porous electrodes, and inhomogeneous boundary layer thickness in flow batteries. Such spatial heterogeneity naturally introduces a distribution of diffusion times, corresponding to the set of internal path lengths. Although this concept has been discussed in different contexts, including batteries [27,32,48,62–64], capacitors [59,65,66], fuel cells [67], and flow batteries [40], a general mathematical framework has not yet been developed to analyze experimental data. One approach is to couple several finite diffusion elements in parallel, as a crude approximation of the true heterogeneity [48,63]. Another approach is to assume a certain, continuous probability distribution function, sometimes based on supplemental observations such as electron microscope images [27,32,62,64–66]. Both approaches, however, require *a priori* knowledge about the nanostructure to properly

choose the number of diffusion elements or the functional form of the distribution, which is usually not available.

In this Letter, we propose the theory of diffusion impedance for random heterogeneous materials based on a distribution of diffusion times (DDT). The innumerable diffusion paths in a nanostructure generally have different diffusion times, which often contribute independently in parallel to the collective diffusion impedance. Then, the generalized diffusion impedance is given by

$$z_{GD}^{-1}(\omega) = \int_0^\infty P(\tau) z_D^{-1}(\omega, \tau) d\tau, \tag{1}$$

where $P(\tau)$ is the DDT and z_D is the finite-length diffusion model that represents the individual diffusion paths, as shown in Table I for a set of representative geometries and boundary conditions. In a circuit analogy, z_{GD} can be represented by an infinite parallel array of z_D, each of which has a different time constant. We present a general method to solve the inverse problem for the DDT from experimental data that does not assume *a priori* knowledge on the configurational randomness and consider three representative cases: a supercapacitor, a Li-ion battery, and a flow battery.

The DDT framework extends the traditional interpretation of impedance spectra in terms of a distribution of relaxation times (DRT) for a linear superposition of the parallel RC circuit elements [68–70]. Recently, DRT analysis has been increasingly applied to electrochemical energy systems [54,71–74], although it is intended only to represent high-frequency interfacial charging and Faradaic reactions. Low-frequency diffusion impedance, which contains geometrical information about transport pathways, is mathematically and physically distinct and cannot be meaningfully represented by a DRT. Instead, the appropriate DDT must be defined.

The geometrical interpretation of the DDT, where each diffusion time $\tau = \ell^2/D$ corresponds to a nanoscale path length ℓ traversed with diffusivity D, suggests a tantalizing possibility of "impedance imaging" of nanostructures, by inverting the impedance spectrum to obtain $P(\tau)$. The inversion problem is a Fredholm integral equation of the first kind, which commonly appears in statistical thermodynamics [75], polymer rheology [76], medical imaging [77], and other fields. Upon a change of variables, such that $t = \log(\tau)$ and $u = -\log(\omega)$, Eq. (1) can be written in a convolution form:

$$y(u) = \int_{-\infty}^\infty K(u - t) q(t) dt, \tag{2}$$

where $y = z_{GD}^{-1}$ is the admittance of the nanostructure, $K = z_D^{-1}$ is the diffusion kernel determined by the diffusion conditions (Table I), and $q(t) = \tau P(\tau)$ is the unknown distribution function. Evaluating at a discrete set of u_n for $n = 1, 2, ..., N$ and discretizing t for a discrete set of t_m for $m = 1, 2, ..., M$, Eq. (2) can be approximated by $\mathbf{y} = \mathbf{KHq}$, where $\mathbf{y}$ and $\mathbf{q}$ are vectors such that $y_n = y(u_n)$ and $q_m = q(t_m)$; $\mathbf{K}$ is a kernel matrix such that $K_{n,m} = K(u_n - t_m)$; and $\mathbf{H}$ is a discretization matrix of the integral, for which we adopt the trapezoidal rule, although other discretization schemes may be used [78]. Given sufficient data, such that $N > M$, finding $\mathbf{q}$ may seem like a simple linear overdetermined problem subject to an inequality constraint $\mathbf{q} \geq 0$. However, this class of inversion problems is known to be mathematically ill posed, and a naïve least squares regression does not provide a reliable solution.

Tikhonov regularization is a common method to solve such an inversion problem [79,80], while others include the lasso regularization [81], the maximum entropy regularization [82,83], the Monte Carlo method [84], and the Fourier transform method followed by filtering [72,85]. Tikhonov regularization is a modified least squares method where the loss function includes a penalty term that regulates one of the derivatives (Sobolev norm) of the solution. Here we opt to control the second derivative in order to smooth the fitting of irregular or noisy data. Given a vector of experimental data, $\mathbf{y}^\varepsilon$, the loss function has the following form:

$$\Phi(\mathbf{q}; \mathbf{y}^\varepsilon, \lambda) = \|\mathbf{W}(\mathbf{y}^\varepsilon - \mathbf{KHq})\|_2^2 + \lambda \|\mathbf{D}_2 \mathbf{q}\|_2^2, \tag{3}$$

where the first term is the conventional sum of residual squares and the second term is the penalty term that imposes smoothness of the solution. Here, $\mathbf{W}$ is the diagonal weighting matrix, and $\mathbf{D}_2$ is the second-order difference matrix that approximates $q''(t)$. λ is the regularization parameter that determines the relative scale of the penalty term. Minimization of $\Phi(\mathbf{q})$ belongs to quadratic programming, and its standard formulation is presented in Supplemental Material [86]. Defining the intermediate solution function by $\mathbf{q}^\lambda(\lambda; \mathbf{y}^\varepsilon) = \arg \min \Phi(\mathbf{q}; \mathbf{y}^\varepsilon, \lambda)$ subject to $\mathbf{q} \geq 0$, it is largely affected by the value of λ; a small λ

TABLE I. z_D for different boundary conditions and symmetries. If a charge transfer reaction is taking place simultaneously, their Gerischer-type derivatives can be used instead.

Boundary condition	Blocking			Transmissive
Symmetry	Planar	Cylindrical	Spherical	Planar
$z_D(\omega, \tau)$	$\dfrac{\coth(\sqrt{i\omega\tau})}{\sqrt{i\omega\tau}}$	$\dfrac{I_0(\sqrt{i\omega\tau})}{\sqrt{i\omega\tau}I_1(\sqrt{i\omega\tau})}$	$\dfrac{\tanh(\sqrt{i\omega\tau})}{\sqrt{i\omega\tau} - \tanh(\sqrt{i\omega\tau})}$	$\dfrac{\tanh(\sqrt{i\omega\tau})}{\sqrt{i\omega\tau}}$

FIG. 1. (a) Artificial spectra (AS1 and AS2) and their model fits (MF1 and MF2, respectively) presented on the complex plane and (b) their phase angles and magnitudes plotted against the frequency. (c) The true normal distribution used in generating AS1 and its estimation by inversion of AS1 and (d) the true bimodal distribution used in generating AS2 and its estimation by inversion of AS2. The error bars indicate 90% statistical errors of the estimations, obtained by the bootstrap resampling method for a given $\hat{\lambda}$ [79].

results in overfitting or oscillation in $\mathbf{q}^{\lambda}$, whereas a large λ results in oversmoothing.

To determine λ, we employed the real-imaginary cross-validation method, where we minimize the prediction errors of separate real and imaginary parts of $\mathbf{y}^{\varepsilon}$ with respect to the other part [81,88]:

$$\Psi(\lambda) = \|\mathbf{W}\{\mathrm{Re}[\mathbf{y}^{\varepsilon}] - \mathrm{Re}[\mathbf{K}\mathbf{H}\mathbf{q}^{\lambda}(\lambda; \mathrm{Im}[\mathbf{y}^{\varepsilon}])]\}\|_2^2$$
$$+ \|\mathbf{W}\{\mathrm{Im}[\mathbf{y}^{\varepsilon}] - \mathrm{Im}[\mathbf{K}\mathbf{H}\mathbf{q}^{\lambda}(\lambda; \mathrm{Re}[\mathbf{y}^{\varepsilon}])]\}\|_2^2. \quad (4)$$

It is an extension of k-fold cross-validation for a complex function, with $k = 2$ partitioning the real and imaginary parts, that is reliable even for a limited number of data. The nested minimization of Ψ provides a self-consistent $\hat{\lambda}$, which then can be used to calculate the final solution, $\hat{\mathbf{q}} = \mathbf{q}^{\lambda}(\hat{\lambda}; \mathbf{y}^{\varepsilon})$. This inversion method leads to an accurate estimation when a smooth, well-behaved solution is expected. Otherwise, the hierarchical regularization method can be employed [89].

We first illustrate the DDT method for artificial spectra generated from a known distribution with noise, using the inversion method to recover the distribution from the spectra. Figure 1 shows two representative results where a normal distribution and a bimodal distribution are accurately determined from the spectra without *a priori*

assumptions about the functional form. Further details of the simulation studies can be found in Supplemental Material [86]. As shown in the bimodal example [Fig. 1(d)], two distinct peaks can be resolved as long as $\Delta \bar{t} \Delta u \ll 1$ for $t_a \leq u_n \leq t_b$, where $\Delta \bar{t}$ is the separation of the peak times $\bar{t}_a$ and $\bar{t}_b$ and Δu is the sampling period among u_n. This uncertainty principle sets the resolution limit for multimodal distributions, e.g., for a battery electrode with a mixture of active materials or a porous electrode with inhomogeneous local nanostructure. Even applying to their aging behavior, it could be possible to separately track the degradation of each part of the nanostructures. This, on the other hand, would be nearly impossible to discern in the impedance spectra, prior to the inverse transform.

For the first physical example, we apply our method to determine the DDT for a vertically aligned carbon nanotube (CNT) supercapacitor from the experiments of Mutha *et al.* [90]. Considering a vertical unit space surrounded by the CNTs, conductive charging of the double layer along the CNT sidewalls can be described by the planar bounded Warburg kernel. The charging time is determined by the length of the tortuous CNTs and the cross-sectional area of the unit space, and their spatial variations lead to a DDT for the charging time. In Figs. 2(a) and 2(b), the DDT model accurately fits spectra that deviate slightly from the ideal bounded Warburg behavior, and the underlying distribution is extracted by the inversion method. We can also see how the distribution changes by experimental variables, such as the volume fraction (V_f) of CNTs as shown in Fig. 2(c). With increasing V_f, up to 15%, the primary distribution shifts to larger values in t. The most probable charging time, $\bar{\tau}$, shows a unit slope with respect to V_f in a log-log plot [Fig. 2(d)], which is predicted theoretically [90]. At a higher volume fraction (26%), however, it shifts back to lower t, which is probably due to CNT bundling that renders the inner sidewalls inaccessible. Secondary peaks are observed in intermediate volume fractions from 2% to 10% as well as at 26%, which is associated with the heavy tails when the distributions are mapped onto the interspacing length Γ in Fig. 2(e). Such an observation was not possible in the previous study assuming a normal distribution [90]. The distributions in Γ obtained from the impedance inversion are consistent with a stochastic simulation [91–93].

For our second example, we perform a DDT analysis of impedance spectra for a silicon nanowire (SiNW) Li-ion battery anode from the work of Chan *et al.* [10] and Ruffo *et al.* [44]. Here, Li$^+$ diffuses radially from the side surface to the center of the nanowires, and the diffusion in individual nanowires is modeled by the cylindrical bounded diffusion kernel [27]. In Figs. 3(a) and 3(b), the DDT model accurately captures its inclined diffusion impedance, and the underlying DDT is determined by the inversion method. In Fig. 3(c), as the nanowires are lithiated, the DDT spreads wider and then narrows back reversively after subsequent delithiation in Fig. 3(d). In Fig. 3(e), the DDTs are
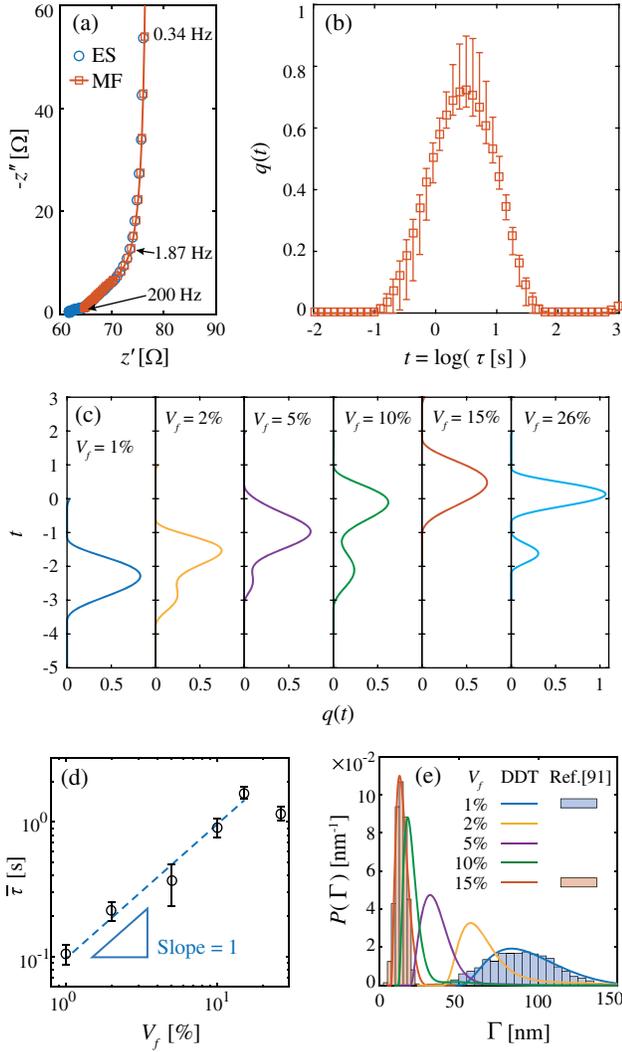
FIG. 2. (a) Experimental spectra (ES) of a CNT electrode and its model fit (MF) at $V_f = 15\%$. (b) The corresponding distribution of time constant estimated by the DDT model. Spectra at other V_f and their inversion results are provided in Supplemental Material [86]. (c) Change in the distribution over a range of V_f and (d) shift in the most probable time constant $\bar{\tau}$ with respect to V_f. (e) Distributions in interspacing length Γ, obtained by the DDT model and by a stochastic simulation [91].

converted to nanowire radius (r) distributions, which show a consistent trend within the experimental observations. Such an estimation could infer the state of health or degradation of the electrode without damaging the cell. The Li$^+$ diffusivity can be estimated by matching either the mean (μ) or the standard deviation (σ) of the radius distribution. The estimated values are presented in Supplemental Material [86]. As shown in Fig. 3(f), the obtained diffusivity varies between 1 and 5×10^{-11} cm^2/s, depending on the concentration, consistent with the results of Dimov et al. [94]. At high concentrations, both approaches result in impressively proximate estimations. On the other hand, the same spectra could result in an overestimation if interpreted by a primitive model [44].
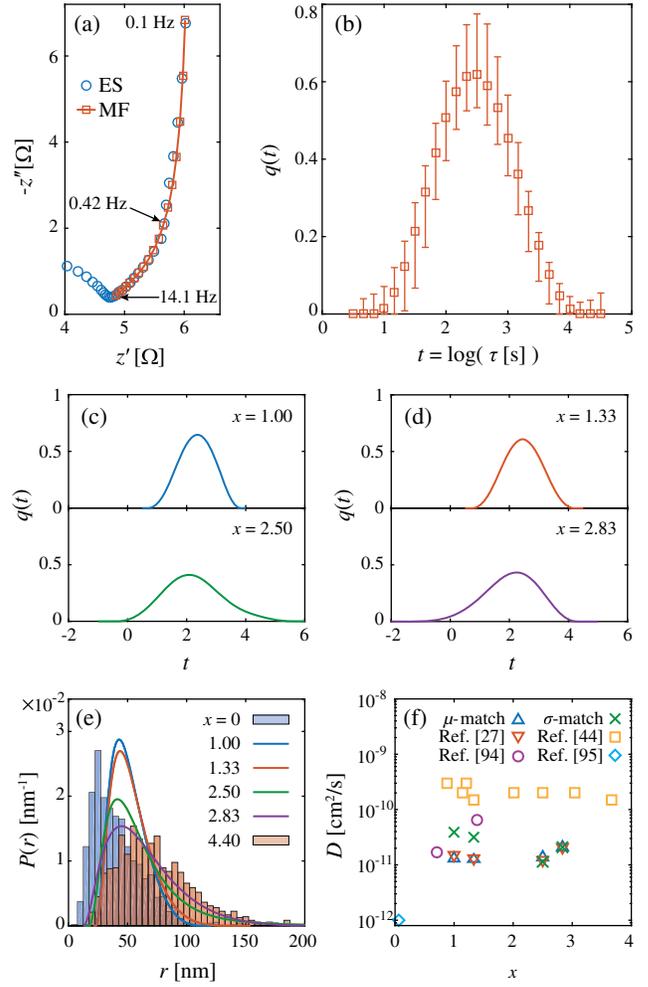
FIG. 3. (a) Experimental spectra (ES) of a SiNW electrode and its model fit (MF) at $x = 1.33$, where x is the stoichiometric concentration of lithium in Li$_x$Si. (b) The corresponding DDT estimated by the inversion method. Spectra at other x and their inversion results are provided in Supplemental Material [86]. (c) DDTs at a low and a high x during lithiation and (d) during subsequent delithiation. (e) Radius distributions obtained by the DDT model (curves) and the SEM image analysis (bars) [10]. (f) Estimated diffusivity and comparison to other studies [27,44,94,95].

Our final example, shown in Fig. 4, is a vanadium flow battery of Liu et al. [96], which illustrates the DDT analysis for transmissive diffusion. As the electrolyte flows through the porous carbon electrode, a boundary layer develops on the microscopic internal surface. The Nernst diffusion layer model leads to the transmissive diffusion kernel in Table I. The boundary layer has spatial variation in its thickness due to the variation in local velocity and pore configuration, which leads to a DDT. In Fig. 4(a), the model shows an excellent agreement with its diffusion impedance, even though the arc is significantly suppressed compared to the ideal finite-length Warburg behavior. The inverted DDT, shown in Fig. 4(b), reveals the dispersion of mass transport rate in a random porous medium, in addition to the mean.
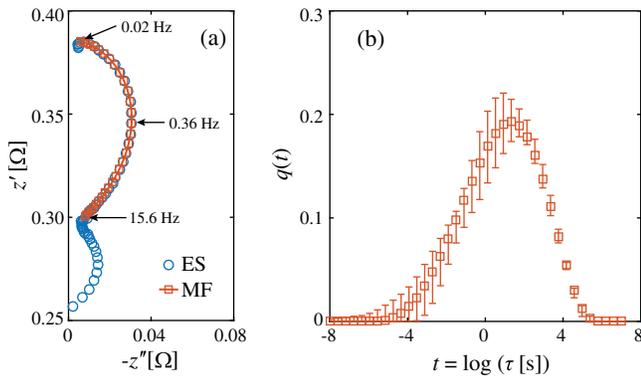
FIG. 4. (a) Experimental spectra (ES) of a vanadium flow battery and its model fit (MF). (b) The corresponding DDT estimated by the inversion method.

A more detailed study with microstructural characterization will follow [97].

In conclusion, we propose a method of impedance analysis that considers the inherent geometrical randomness of diffusion in nanostructured materials, including (but not limited to) advanced porous electrodes for energy storage. It extends the traditional finite Warburg and Gerischer circuit elements by incorporating the DDT. We have also developed a mathematical framework to determine the DDT from electrochemical impedance spectra and demonstrated the possibility of impedance imaging for different types of nanostructured electrodes.

The method is not limited to purely diffusive processes but could be extended for reaction-diffusion phenomena in heterogeneous materials. For example, the model with a Gerischer-type kernel could be applied to impedance spectra for solid oxide fuel cells, in order to more accurately extract the surface diffusivity and adsorption rate constant for oxygen electrocatalysis by accounting for the observed statistical variations in the functional layer microstructure [34,35,53,98]. Also, the DDT model can be combined with the traditional DRT model to transform impedance spectra of the entire frequency range. Our numerical inversion method could be applied to the hybrid DDT and DRT models as well to simultaneously study the dispersion of low-frequency bulk diffusion and high-frequency interfacial charging and reactions.

---

[*]bazant@mit.edu

[1] A. S. Arico, P. Bruce, B. Scrosati, J.-M. Tarascon, and W. van Schalkwijk, Nat. Mater. **4**, 366 (2005).

[2] Y.-G. Guo, J.-S. Hu, and L.-J. Wan, Adv. Mater. **20**, 2878 (2008).

[3] A. Manthiram, A. V. Murugan, A. Sarkar, and T. Muraliganth, Energy Environ. Sci. **1**, 621 (2008).

[4] M. C. Orilall and U. Wiesner, Chem. Soc. Rev. **40**, 520 (2011).

[5] L. Ji, Z. Lin, M. Alcoutlabi, and X. Zhang, Energy Environ. Sci. **4**, 2682 (2011).

[6] X. Ji, K. T. Lee, and L. F. Nazar, Nat. Mater. **8**, 500 (2009).

[7] B. Kang and G. Ceder, Nature (London) **458**, 190 (2009).

[8] K. T. Nam, D.-W. Kim, P. J. Yoo, C.-Y. Chiang, N. Meethong, P. T. Hammond, Y.-M. Chiang, and A. M. Belcher, Science **312**, 885 (2006).

[9] J. R. Szczech and S. Jin, Energy Environ. Sci. **4**, 56 (2011).

[10] C. K. Chan, H. Peng, G. Liu, K. McIlwrath, X. F. Zhang, R. A. Huggins, and Y. Cui, Nat. Nanotechnol. **3**, 31 (2008).

[11] W. Chen, R. Rakhi, L. Hu, X. Xie, Y. Cui, and H. N. Alshareef, Nano Lett. **11**, 5165 (2011).

[12] H. Jiang, P. S. Lee, and C. Li, Energy Environ. Sci. **6**, 41 (2013).

[13] G. Yu, X. Xie, L. Pan, Z. Bao, and Y. Cui, Nano Energy **2**, 213 (2013).

[14] Z. Yu, L. Tetard, L. Zhai, and J. Thomas, Energy Environ. Sci. **8**, 702 (2015).

[15] M. Zhi, C. Xiang, J. Li, M. Li, and N. Wu, Nanoscale **5**, 72 (2013).

[16] Y. Liu, S. Zha, and M. Liu, Adv. Mater. **16**, 256 (2004).

[17] Y. Qiao and C. M. Li, J. Mater. Chem. **21**, 4027 (2011).

[18] Z. Zhan, D. M. Bierschenk, J. S. Cronin, and S. A. Barnett, Energy Environ. Sci. **4**, 3951 (2011).

[19] C.-J. Zhong, J. Luo, B. Fang, B. N. Wanjala, P. N. Njoki, R. Loukrakpam, and J. Yin, Nanotechnology **21**, 062001 (2010).

[20] Z. González, S. Vizireanu, G. Dinescu, C. Blanco, and R. Santamaría, Nano Energy **1**, 833 (2012).

[21] M. Park, J. Ryu, and J. Cho, Chem. Asian J. **10**, 2096 (2015).

[22] Y. Shao, Y. Cheng, W. Duan, W. Wang, Y. Lin, Y. Wang, and J. Liu, ACS Catal. **5**, 7288 (2015).

[23] E. Barsoukov and J. R. Macdonald, *Impedance Spectroscopy: Theory, Experiment, and Applications* (Wiley, New York, 2005).

[24] M. E. Orazem and B. Tribollet, *Electrochemical Impedance Spectroscopy* (Wiley, New York, 2011), Vol. 48.

[25] J. Bisquert, J. Phys. Chem. B **106**, 325 (2002).

[26] C. Ho, I. Raistrick, and R. Huggins, J. Electrochem. Soc. **127**, 343 (1980).

[27] J. Song and M. Z. Bazant, J. Electrochem. Soc. **160**, A15 (2013).

[28] P. Drossbach, Electrochim. Acta **11**, 667 (1966).

[29] P. Drossbach and J. Schulz, Electrochim. Acta **9**, 1391 (1964).

[30] J. Ross Macdonald, J. Electroanal. Chem. Interfacial Electrochem. **32**, 317 (1971).

[31] D. R. Franceschetti and J. R. Macdonald, J. Electrochem. Soc. **129**, 1754 (1982).

[32] J. Song and M. Z. Bazant, Electrochim. Acta **131**, 214 (2014).

[33] B. Boukamp, M. Verbraeken, D. Blank, and P. Holtappels, Solid State Ionics **177**, 2539 (2006).

[34] Y. Fu, S. Poizeau, A. Bertei, C. Qi, A. Mohanram, J. Pietras, and M. Bazant, Electrochim. Acta 159, 71 (2015).

[35] J. Nielsen, T. Jacobsen, and M. Wandel, Electrochim. Acta 56, 7963 (2011).

[36] R. de Levie, Electrochim. Acta 8, 751 (1963).

[37] A. Lasia, J. Electroanal. Chem. 397, 27 (1995).

[38] D. Han, X. Liu, F. Zeng, J. Qian, T. Wu, and Z. Zhan, Sci. Rep. 2, 462 (2012).

[39] B. Liu, H. Muroyama, T. Matsui, K. Tomida, T. Kabata, and K. Eguchi, J. Electrochem. Soc. 158, B215 (2011).

[40] C.-N. Sun, F. M. Delnick, D. S. Aaron, A. B. Papandrew, M. M. Mench, and T. A. Zawodzinski, J. Electrochem. Soc. 161, A981 (2014).

[41] F. Fabregat-Santiago, G. Garcia-Belmonte, J. Bisquert, N. S. Ferriols, P. R. Bueno, E. Longo, J. S. Antón, and S. Castro-García, J. Electrochem. Soc. 148, E302 (2001).

[42] J. García-Cañadas, F. Fabregat-Santiago, I. Porqueras, C. Person, J. Bisquert, and G. Garcia-Belmonte, Solid State Ionics 175, 521 (2004).

[43] A. Lundqvist and G. Lindbergh, Electrochim. Acta 44, 2523 (1999).

[44] R. Ruffo, S. S. Hong, C. K. Chan, R. A. Huggins, and Y. Cui, J. Phys. Chem. C 113, 11390 (2009).

[45] L. O. Valøen, S. Sunde, and R. Tunold, J. Alloys Compd. 253–254, 656 (1997).

[46] J. Bisquert, G. Garcia-Belmonte, P. Bueno, E. Longo, and L. Bulhoes, J. Electroanal. Chem. 452, 229 (1998).

[47] A. Funabiki, M. Inaba, Z. Ogumi, S. i. Yuasa, J. Otsuji, and A. Tasaka, J. Electrochem. Soc. 145, 172 (1998).

[48] T. Osaka, T. Momma, D. Mukoyama, and H. Nara, J. Power Sources 205, 483 (2012).

[49] R. de Levie, J. Electroanal. Chem. Interfacial Electrochem. 281, 1 (1990).

[50] L. Nyikos and T. Pajkossy, Electrochim. Acta 30, 1533 (1985).

[51] T. Kaplan, L. J. Gray, and S. H. Liu, Phys. Rev. B 35, 5379 (1987).

[52] B. A. Boukamp, M. Verbraeken, D. H. A. Blank, and P. Holtappels, Solid State Ionics 177, 2539 (2006).

[53] J. Nielsen and J. Hjelm, Electrochim. Acta 115, 31 (2014).

[54] J. P. Schmidt, T. Chrobak, M. Ender, J. Illig, D. Klotz, and E. Ivers-Tiffée, J. Power Sources 196, 5342 (2011).

[55] R. Cabanel, G. Barral, J.-P. Diard, B. Le Gorrec, and C. Montella, J. Appl. Electrochem. 23, 93 (1993).

[56] J. Bisquert, G. Garcia-Belmonte, F. Fabregat-Santiago, N. S. Ferriols, P. Bogdanoff, and E. C. Pereira, J. Phys. Chem. B 104, 2287 (2000).

[57] J. Bisquert, G. Garcia-Belmonte, and Á. Pitarch, ChemPhysChem 4, 287 (2003).

[58] L. M. Gassa, J. R. Vilche, M. Ebert, K. Jüttner, and W. J. Lorenz, J. Appl. Electrochem. 20, 677 (1990).

[59] M. Eikerling, A. Kornyshev, and E. Lust, J. Electrochem. Soc. 152, E24 (2005).

[60] J. Bisquert, Phys. Rev. Lett. 91, 010602 (2003).

[61] J. Bisquert and A. Compte, J. Electroanal. Chem. 499, 112 (2001).

[62] J. P. Diard, B. Le Gorrec, and C. Montella, J. Electroanal. Chem. 499, 67 (2001).

[63] M. D. Levi and D. Aurbach, J. Phys. Chem. B 108, 11693 (2004).

[64] J. P. Meyers, M. Doyle, R. M. Darling, and J. Newman, J. Electrochem. Soc. 147, 2930 (2000).

[65] H.-K. Song, H.-Y. Hwang, K.-H. Lee, and L. H. Dao, Electrochim. Acta 45, 2241 (2000).

[66] H.-K. Song, Y.-H. Jung, K.-H. Lee, and L. H. Dao, Electrochim. Acta 44, 3513 (1999).

[67] J. Nielsen, T. Jacobsen, and M. Wandel, Electrochim. Acta 56, 7963 (2011).

[68] G. Brug, A. Van Den Eeden, M. Sluyters-Rehbach, and J. Sluyters, J. Electroanal. Chem. Interfacial Electrochem. 176, 275 (1984).

[69] B. Hirschorn, M. E. Orazem, B. Tribollet, V. Vivier, I. Frateur, and M. Musiani, J. Electrochem. Soc. 157, C452 (2010).

[70] J. R. Macdonald, J. Appl. Phys. 61, 700 (1987).

[71] J. Illig, M. Ender, A. Weber, and E. Ivers-Tiffée, J. Power Sources 282, 335 (2015).

[72] H. Schichlein, A. C. Müller, M. Voigts, A. Krügel, and E. Ivers-Tiffée, J. Appl. Electrochem. 32, 875 (2002).

[73] J. P. Schmidt, P. Berg, M. Schönleber, A. Weber, and E. Ivers-Tiffée, J. Power Sources 221, 70 (2013).

[74] A. Weiß, S. Schindler, S. Galbiati, M. A. Danzer, and R. Zeis, Electrochim. Acta 230, 391 (2017).

[75] M. Z. Bazant and B. L. Trout, Physica (Amsterdam) 300A, 139 (2001).

[76] J. Honerkamp and J. Weese, Rheol. Acta 32, 65 (1993).

[77] Y. M. Kadah and X. Hu, IEEE Trans. Med. Imaging 17, 362 (1998).

[78] T. H. Wan, M. Saccoccio, C. Chen, and F. Ciucci, Electrochim. Acta 184, 483 (2015).

[79] J. Honerkamp and J. Weese, Continuum Mech. Thermodyn. 2, 17 (1990).

[80] H. Schäfer, E. Sternin, R. Stannarius, M. Arndt, and F. Kremer, Phys. Rev. Lett. 76, 2177 (1996).

[81] M. Saccoccio, T. H. Wan, C. Chen, and F. Ciucci, Electrochim. Acta 147, 470 (2014).

[82] U. Amato and W. Hughes, Inverse Probl. 7, 793 (1991).

[83] L. R. Mead, J. Math. Phys. 27, 2903 (1986).

[84] E. Tuncer and J. R. Macdonald, J. Appl. Phys. 99, 074106 (2006).

[85] B. A. Boukamp, Electrochim. Acta 154, 35 (2015).

[86] See Supplemental Material at http://link.aps.org/supplemental/10.1103/PhysRevLett.120.116001 for the standard form of the quadratic programming, the detail specifications of the simulation studies, and more spectra and inversion results for the CNT supercapacitor and the SiNW Li-ion battery electrodes, as well as the estimated diffusivity of Li^+ in SiNWs, which includes Ref. [87].

[87] J. Nocedal and S. Wright, Numerical Optimization (Springer Science, New York, 2006).

[88] J. Macutkevic, J. Banys, and A. Matulis, Nonlinear Anal. Model. Control 9, 75 (2004).

[89] F. Ciucci and C. Chen, Electrochim. Acta 167, 439 (2015).

[90] H. K. Mutha, Y. Lu, I. Y. Stein, H. J. Cho, M. E. Suss, T. Laoui, C. V. Thompson, B. L. Wardle, and E. N. Wang, Nanotechnology 28, 05LT01 (2017).

[91] I. Y. Stein and B. L. Wardle, Phys. Chem. Chem. Phys. 18, 694 (2016).

[92] I. Y. Stein, D. J. Lewis, and B. L. Wardle, Nanoscale **7,** 19426 (2015).

[93] I. Y. Stein and B. L. Wardle, Phys. Chem. Chem. Phys. **15,** 4033 (2013).

[94] N. Dimov, K. Fukuda, T. Umeno, S. Kugino, and M. Yoshio, J. Power Sources **114,** 88 (2003).

[95] G. A. Tritsaris, K. Zhao, O. U. Okeke, and E. Kaxiras, J. Phys. Chem. C **116,** 22212 (2012).

[96] S. Liu, M. Kok, Y. Kim, J. L. Barton, F. R. Brushett, and J. Gostick, J. Electrochem. Soc. **164,** A2038 (2017).

[97] J. L. Barton, J. Song, M. Z. Bazant, and F. R. Brushett (to be published).

[98] E.-C. Shin, P.-A. Ahn, H.-H. Seo, J.-M. Jo, S.-D. Kim, S.-K. Woo, J. H. Yu, J. Mizusaki, and J.-S. Lee, Solid State Ionics **232,** 80 (2013).